Direct Harmonic Analysis of the Voltage Source Converter

Peter W. Lehn, *Member, IEEE*

***Abstract*—An analytic technique is presented for the calculation of both characteristic and uncharacteristic harmonics in voltage source converter circuits. The proposed technique accounts for all harmonic interaction between the ac and dc sides of the converter, and may thus also be employed for accurate dc side voltage ripple calculations. In contrast to simulation-based approaches or iterative methods, the proposed technique offers a closed form solution for the current harmonics, thereby avoiding numerical errors and convergence problems. The technique is applied to the harmonic analysis of a STATCOM.**

***Index Terms*—FACTS, harmonic analysis, pulsewidth modulation, STATCOM.**

I. Introduction

THE INTRODUCTION of VSC-based FACTS equipment to a power system offers the potential to improve control of power flow and enhance system stability. As with any VSC application, converter-based FACTS equipment will act as a source of harmonic current injection to the system and it will also interact with harmonic distortions already present within the system. In order to prevent harmonic instability of the system and to appropriately rate the components of the VSC, an improved understanding of these harmonic interactions must be developed.

Two established techniques exist for performing an approximate analysis of the behavior of FACTS components at frequencies away from the fundamental. In [1], [2], the modeling of a converter under unbalanced operating conditions is carried out by representing switching functions by their Fourier Spectra. Iterative techniques can then be applied to perform a harmonic balance. This approach has the potential to offer an accurate solution, accounting for all harmonics and harmonic interactions within the system; however, the complexity in the approach increases rapidly with the number of harmonics being considered. Furthermore, this approach requires an iterative solution technique to be employed, which requires convergence conditions to be met.

An alternate type of approach is presented in [3], [4], and [5] where dq-frame converter models are employed as a basis for analyzing the converter. These techniques are more straightforward than those which model the switching functions, but they are bandwidth limited and not capable of modeling harmonic sidebands introduced around the carrier frequency of the pulsewidth modulator.

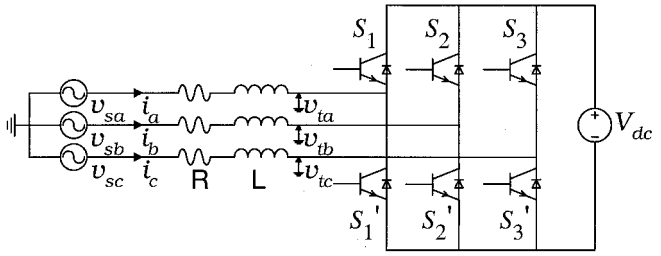

Fig. 1. VSC circuit.

This paper presents a direct analytical method to calculate the harmonics in a VSC circuit. Balanced and unbalanced operating conditions are considered where unbalance may stem from either system voltage or converter firing unbalance. The presented technique calculates all characteristic and uncharacteristic harmonics of the converter, accounting for all harmonic coupling through the dc link of the converter. The technique may be used to analyze the harmonic response of any VSC-based equipment including FACTS components such as the STATCOM and SSSC. Straightforward extensions to the technique permits application to multiterminal VSC-based FACTS equipment such as the UPFC or IPFC.

The paper is divided into five main sections. First, the concept of space vector-based harmonic analysis is presented with the help of a simple example, assuming a ripple free dc bus. Second, using space vector concepts, an analytical solution is developed for complete harmonic analysis of a converter, including all ac-dc side interactions. Next, the proposed technique is validated against PSCAD/EMTDC simulation results and the computational benefits of implementing the technique are assessed. Finally, a complete harmonic analysis of a STATCOM is carried out to demonstrate one possible application of the proposed theory.

II. Space Vector Harmonic Analysis

Consider the converter of Fig. 1 operating under sinusoidal pulsewidth modulation (SPWM). For proper SPWM operation, the carrier frequency of the modulator is an odd multiple of three times the fundamental system frequency [6]. Thus

$$f_{carrier} = 3nf_{system} \qquad n = odd. \tag{1}$$

Fig. 2 shows the phase a system voltage and the converter gating signals for the case $n = 1$. For $n = 1$ three switching

Manuscript received September 25, 2002.

The author is with the Department of Electrical and Computer Engineering, University of Toronto, Toronto, ON M5S 3G4, Canada (e-mail: lehn@power.ele.utoronto.ca).

Digital Object Identifier 10.1109/TPWRD.2003.813603

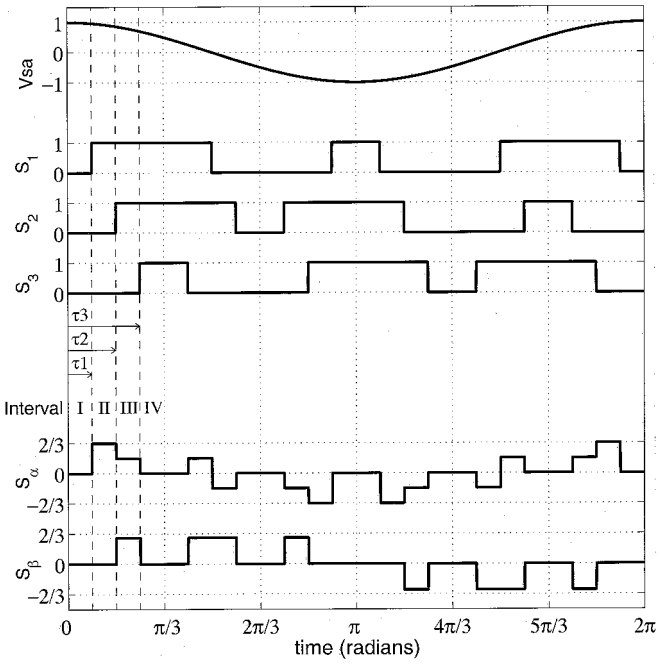

Fig. 2. VSC gating signals.

events (τ_1, τ_2, τ_3) may be identified every 60° of the fundamental. In general, $3n$ switching events will occur every 60°.

Balanced three-phase operation of the system implies that the following four conditions are met.

- AC source is balanced.
- Interface impedances in the phases are all identical.
- Switch-on times are equally spaced throughout the period (i.e., every 60°).
- All switch-off times are equally spaced throughout the period (i.e., every 60°).

Under these conditions, 60° symmetry will exist in the voltage and current waveforms.

To best exploit this symmetry, analysis of the system is carried out in the $\alpha\beta$ reference frame. Voltages, currents, and gating signals are all transformed into the $\alpha\beta$-frame through a variation of the Clarke Transform [7], [8]. The transform is applied to the gating signals according to

$$\begin{bmatrix} S_\alpha \\ S_\beta \end{bmatrix} = \tfrac{2}{3}\,\mathbf{C_x} \begin{bmatrix} S_1 \\ S_2 \\ S_3 \end{bmatrix} \tag{2}$$

where

$$\mathbf{C_x} = \begin{bmatrix} 1 & -\frac{1}{2} & -\frac{1}{2} \\ 0 & \frac{\sqrt{3}}{2} & -\frac{\sqrt{3}}{2} \end{bmatrix}. \tag{3}$$

The inverse of the $(2/3)\mathbf{C_x}$ Transform is simply given by ${\mathbf{C_x}}^T$ where the superscript T denotes transpose. As shown in Fig. 2, the $\alpha\beta$-frame gating signals take on a multilevel waveform.

Assuming the dc voltage is constant, ripple free and of amplitude V_{dc}, then the terminal voltage of the converter in the $\alpha\beta$-frame is given by

$$\begin{bmatrix} v_{t\alpha} \\ v_{t\beta} \end{bmatrix} = \begin{bmatrix} S_\alpha \\ S_\beta \end{bmatrix} V_{dc} \tag{4}$$

where voltages are either given directly in volts, or given in per unit using the base value convention specified in the Appendix.

Space vector-based harmonic analysis of the converter voltage is then carried out by performing a complex Fourier analysis on the converter terminal's complex voltage vector $\vec{v_t} = v_{t\alpha} + jv_{t\beta}$. The positive sequence fundamental component of this vector will rotate in a clockwise direction, making a single complete revolution in one period. On a normalized time base, the positive sequence component is thus found from

$$\vec{V_t}^{+1} = \frac{1}{2\pi}\int_0^{2\pi} (v_{t\alpha} + jv_{t\beta})e^{-jt}\,dt. \tag{5}$$

From symmetry, this may be reduced to a sixth period analysis. For $n = 1$, the vector $\vec{v_t}$ takes on four discrete values associated with the four intervals marked in Fig. 2, yielding a positive sequence component which depends on the switching instants and the dc voltage

$$\vec{V_t}^{+1} = \frac{3}{\pi}\left(\int_{\tau_1}^{\tau_2} \frac{2}{3}\,V_{dc}e^{-jt}\,dt + \int_{\tau_2}^{\tau_3} \frac{2}{3}\,e^{j\pi/3}V_{dc}e^{-jt}\,dt\right). \tag{6}$$

All other characteristic harmonics may also be found from the sixth period analysis. Let h represent the harmonic number in question, where positive h values correspond to positive sequence harmonics and negative h values to negative sequence harmonics. The hth harmonic component of the converter terminal voltage may thus be found from

$$\vec{V_t}^{h} = \frac{3}{\pi}\left(\int_{\tau_1}^{\tau_2} \frac{2}{3}\,V_{dc}e^{-jht}\,dt + \int_{\tau_2}^{\tau_3} \frac{2}{3}\,e^{j\pi/3}V_{dc}e^{-jht}\,dt\right) \tag{7}$$

for $h = -5, +7, -11, +13\cdots$.

The hth harmonic current is found via traditional phasor analysis and is given by

$$\vec{I}^{h} = \frac{\vec{V_s}^{h} - \vec{V_t}^{h}}{R + j|h|L} \tag{8}$$

where $\vec{V_s}^{h}$ is the hth harmonic component of the system bus voltage.

Since, in this case, the dc voltage is held constant by a dc source, the converter may be run at an arbitrary modulation index and delay angle. Fig. 3 shows the complex spectrum of the current space vector for a system running with a modulation index of $m_a = 0.9$ p.u., a delay angle $\delta = 3°$ and a dc voltage of 2.1 p.u. (i.e., 2.1 times the peak line to neutral voltage of the ac system). The system parameters are given in the Appendix.

Analysis of the complex space vector yields an asymmetric spectrum, where negative sequence components appear in the left half plane and positive sequence components appear in the right half plane. The corresponding spectrum obtained from a PSCAD/EMTDC simulation is also shown. The simulated spectrum is determined by Fourier analysis of the three line currents followed by decomposition into sequence components. If a suf-

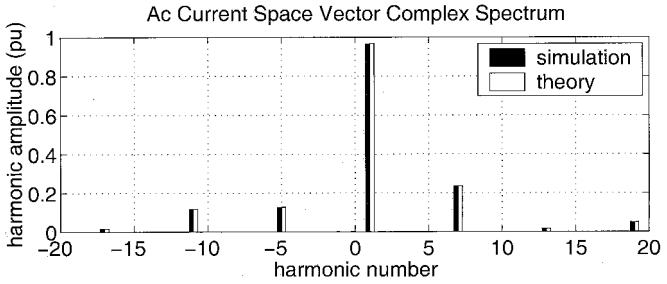

Fig. 3. Complex harmonic spectrum of the VSC ac current assuming a fixed dc voltage level for $f_{carrier} = 3f_{system}$.

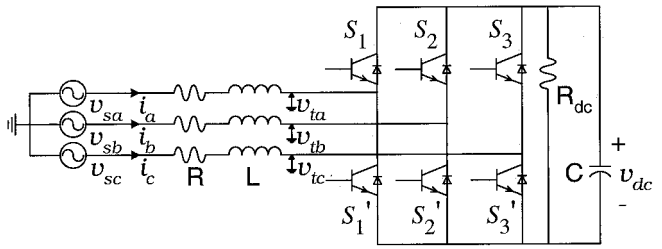

Fig. 4. VSC with dc storage capacitor.

ficiently small time step is employed for the simulation, results are identical.

III. Complete Harmonic Analysis

In practice, the majority of converters are not run off a constant dc voltage source, but are instead designed using a dc side capacitor as shown in Fig. 4. The average steady state dc voltage level is then a function of the modulation index m_a and delay angle δ of the SPWM signal. Furthermore, harmonics will now appear on the dc capacitor voltage, thus it is no longer permissible to assume V_{dc} is constant over the entire period as was done in the preceding analysis.

To model the ac side converter harmonics for the circuit of Fig. 4, requires the following.

- A true steady state solution must be found which takes into account all harmonic interactions, not just fundamental frequency components.
- The current space vector and its harmonics must be determined, taking into account the ripple on the dc capacitor voltage.

An extensive analysis of the steady state operating characteristics of the converter shown in Fig. 4 is presented in [8]. Using a similar development, the system equations may be derived in the $\alpha\beta$-frame

$$\frac{d}{dt}\begin{bmatrix} i_\alpha \\ i_\beta \\ v_{dc} \\ z_1 \\ z_2 \end{bmatrix} = \left[\begin{array}{ccc|cc} -\frac{R}{L} & 0 & -\frac{1}{L}S_\alpha & \frac{1}{L} & 0 \\ 0 & -\frac{R}{L} & -\frac{1}{L}S_\beta & 0 & \frac{1}{L} \\ \hline \frac{3}{2C}S_\alpha & \frac{3}{2C}S_\beta & -\frac{1}{R_{dc}C} & 0 & 0 \\ 0 & 0 & 0 & 0 & -\omega \\ 0 & 0 & 0 & \omega & 0 \end{array}\right] \begin{bmatrix} i_\alpha \\ i_\beta \\ v_{dc} \\ z_1 \\ z_2 \end{bmatrix}. \tag{9}$$

The system voltage has been represented by an ideal oscillator described by the states z_1 and z_2 oscillating at a normalized frequency of $\omega = 1$ p.u. The upper right 2×2 sub-matrix of the system determines how the oscillator is coupled into the VSC differential equations. As shown, the oscillator applies a balanced three-phase voltage to the VSC by applying a cosine wave to the α-axis and a sine wave to the β axis. Section III-C describes how this coupling matrix may be adjusted to model an unbalanced system voltage.

The $\alpha\beta$-frame switching functions in (9) are related to the actual switching functions S_1, S_2, S_3 according to (2). The same transform $(2/3)\mathbf{C_x}$ also relates voltages and currents in the abc-frame to those in the $\alpha\beta$-frame.

At any given instant, the switching functions S_1, S_2, S_3 take on a fixed set of binary values, and associated with this set is a corresponding gating space vector $S_\alpha + jS_\beta$. Equation (9) is then written in compact form by either

$$\frac{d}{dt}\mathbf{x} = \mathbf{A_{S_1S_2S_3}x} \tag{10}$$

or equivalently

$$\frac{d}{dt}\mathbf{x} = \mathbf{A_{S_\alpha + jS_\beta}x}. \tag{11}$$

The system is linear, but its $\mathbf{A}$ matrix is time varying. A steady state does, however, exist, since the time varying nature of $\mathbf{A}$ is periodic. Applying the steady state solution technique [8] yields the initial condition $\mathbf{x_{ss}(0)}$, associated with a steady state solution.

A. Balanced Operation

Sixth period symmetry is exploited to find the system steady state and the characteristic voltage and current harmonics of the converter. Space vectors are used to analyze the harmonic spectrum of the converter current, since they simultaneously identify harmonic amplitude, phase, and sequence. The integral to be solved for the hth harmonic component of the current is

$$\vec{I}^h = \frac{3}{\pi}\int_o^{\pi/3} \vec{i}(t)e^{-jht}\,dt \tag{12}$$

where $\vec{i}(t) = i_\alpha(t) + ji_\beta(t)$.

To solve this equation, the following complex state equation is augmented to the system equations:

$$\frac{dy}{dt} = Ey + F\vec{i}. \tag{13}$$

This equation will be solved with the system equations over a sixth period [9]. At the end of the sixth period, the output will be

$$y\left(\frac{\pi}{3}\right) = e^{E\pi/3}y(0) + \int_0^{\pi/3} e^{-Et}\left(e^{E\pi/3}F\right)\vec{i}(t)\,dt. \tag{14}$$

Comparing (12) with (14), it may be seen that the output $y(\pi/3)$ will yield the hth harmonic of the converter current if the following assignments are made:

$$y(0) = 0$$
$$E = jh$$
$$F = \frac{3}{\pi}e^{-jh\pi/3}.$$

Finding the system harmonics is a three stage process. First, the steady state initial condition $\mathbf{x_{ss}}(0)$ of the original system must be found. Second, the system matrix is augmented with one additional equation for each harmonic of interest. Third, the analytical solution for the augmented system is found at time $t = \pi/3$ by solution of the augmented state equations. The solutions for the augmented states then yield the harmonic components of interest.

Equating the hth harmonic of the converter current requires solution of the following matrix equation at time $t = \pi/3$ starting from the initial condition vector $[\mathbf{x}(0) \quad y_h(0)]^T = [\mathbf{x_{ss}}(0) \quad 0]^T$

$$\frac{d}{dt}\begin{bmatrix}\mathbf{x}\\ y_h\end{bmatrix} = \begin{bmatrix}\mathbf{A_{S_1S_2S_3}} & \mathbf{0}\\ \mathbf{G} & \mathbf{H}\end{bmatrix}\begin{bmatrix}\mathbf{x}\\ y_h\end{bmatrix}. \tag{15}$$

The $\mathbf{G}$ matrix couples the system waveforms to be analyzed into the augmented equations, while the $\mathbf{H}$ matrix simply identifies the harmonic numbers of interest. For extraction of the hth current harmonic, the two matrices are given below

$$\mathbf{G} = \left[\frac{3}{\pi}e^{-jh\pi/3} \quad j\frac{3}{\pi}e^{-jh\pi/3} \quad 0 \quad 0 \quad 0\right] \tag{16}$$

$$\mathbf{H} = [jh]. \tag{17}$$

Expressing (15) as $(d/dt)\hat{\mathbf{x}} = \hat{\mathbf{A}}_{S_1S_2S_3}\hat{\mathbf{x}}$, the solution for the hth harmonic of the current, given by $y_h(\pi/3)$, is simply the last element of the vector

$$\begin{aligned}\hat{\mathbf{x}}(\pi/3) = {} & e^{\hat{\mathbf{A}}_{111}((\pi/3)-\tau_{3n})}e^{\hat{\mathbf{A}}_{110}(\tau_{3n}-\tau_{3n-1})}e^{\hat{\mathbf{A}}_{100}(\tau_{3n-1}-\tau_{3n-2})}\\ & \cdot e^{\hat{\mathbf{A}}_{000}(\tau_{3n-2}-\tau_{3n-3})}e^{\hat{\mathbf{A}}_{100}(\tau_{3n-3}-\tau_{3n-4})}\cdots\\ & \cdot e^{\hat{\mathbf{A}}_{111}(\tau_4-\tau_3)}e^{\hat{\mathbf{A}}_{110}(\tau_3-\tau_2)}e^{\hat{\mathbf{A}}_{100}(\tau_2-\tau_1)}\\ & \cdot e^{\hat{\mathbf{A}}_{000}(\tau_1)}\hat{\mathbf{x}}(0)\end{aligned} \tag{18}$$

when $\hat{\mathbf{x}}(0) = [\mathbf{x_{ss}}(0) \quad 0]^T$.

DC voltage harmonics may be found in an analogous fashion, through further state augmentation.

B. Operation Under Unbalanced Gating

Unbalanced operation may result from either an unbalanced system voltage or unbalanced gating of the VSC. These two cases are treated separately, since the mechanisms at work couple into the system equations in very different ways. In both cases, however, uncharacteristic harmonics are created which have only half wave symmetry. Sixth period symmetry is therefore destroyed, increasing the computational burden and complexity of the solution technique.

Operation under unbalanced firing with a balanced system voltage more closely resembles balanced operation. It will therefore be analyzed first. Unbalanced gating may result from errors in the gating generation unit, imbalance in signals coming from the VSC controller, or imbalance in sensor gains.

Unbalanced gating requires a new steady state initial condition to be found for the system over half a period, followed by state augmentation. Over half a period $9n$ switching events will occur. From the half period steady state solution, the harmonics are therefore solved over a half period according to

$$\begin{aligned}\hat{\mathbf{x}}(\pi) = {} & e^{\hat{\mathbf{A}}_{111}(\pi-\tau_{9n})}e^{\hat{\mathbf{A}}_{011}(\tau_{9n}-\tau_{9n-1})}e^{\hat{\mathbf{A}}_{010}(\tau_{9n-1}-\tau_{9n-2})}\\ & \cdot e^{\hat{\mathbf{A}}_{000}(\tau_{9n-2}-\tau_{9n-3})}e^{\hat{\mathbf{A}}_{010}(\tau_{9n-3}-\tau_{9n-4})}\cdots\\ & \cdot e^{\hat{\mathbf{A}}_{111}(\tau_4-\tau_3)}e^{\hat{\mathbf{A}}_{110}(\tau_3-\tau_2)}e^{\hat{\mathbf{A}}_{100}(\tau_2-\tau_1)}\\ & \cdot e^{\hat{\mathbf{A}}_{000}(\tau_1)}\hat{\mathbf{x}}(0)\end{aligned} \tag{19}$$

when $\hat{\mathbf{x}}(0) = [\mathbf{x_{ss}}(0) \quad 0]^T$.

As may be identified from (19), a nonlinear relation exists between switching instants $\tau_1 \cdots \tau_{9n}$ and the harmonics, contained in last rows of $\hat{\mathbf{x}}(\pi)$.

It may be concluded that the VSC current harmonics will not vary linearly with imbalance in the gating signals.

C. Operation Under Unbalanced Voltage

Introduction of an unbalanced system voltage may be carried out by adjusting elements (1,4), (1,5), (2,4), and (2,5) of the $\mathbf{A}$-matrix in (9) and (15).

Equation (9) shows a system $\mathbf{A}$ matrix with elements (1,4) and (2,5) that couple the ideal oscillator equations to the dynamic equations of the VSC. The space vector voltage applied to the VSC is

$$\vec{v_s}(t) = V_s e^{j\omega t} \tag{20}$$

where the amplitude V_s is determined by the initial condition $[z_1(0) \quad z_2(0)]^T = [V_s \quad 0]^T$ as per [8]. Thus, a cosine of amplitude V_s is applied to the α-axis VSC equation and a sine of amplitude V_s is applied to the β-axis equation.

Under imbalance, a negative sequence voltage vector is added to the $\vec{v_s}(t)$ space vector. This additional vector has amplitude V_{sn} and phase ϕ_n

$$\vec{v_s}(t) = V_s e^{j\omega t} + V_{sn}e^{-j\omega t+\phi_n}. \tag{21}$$

Incorporating these changes into the system $\mathbf{A}$ matrix requires the following assignments:

$$\begin{bmatrix}\mathbf{A}_{14} & \mathbf{A}_{15}\\ \mathbf{A}_{24} & \mathbf{A}_{25}\end{bmatrix} = \frac{1}{L}\begin{bmatrix}1+\dfrac{V_{sn}}{V_s}\cos(\phi_n) & \dfrac{V_{sn}}{V_s}\sin(\phi_n)\\ \dfrac{V_{sn}}{V_s}\sin(\phi_n) & 1-\dfrac{V_{sn}}{V_s}\cos(\phi_n)\end{bmatrix}. \tag{22}$$

Using the above modifications to the $\mathbf{A}$ matrix, the system steady state may be found over half a period including the effects of negative sequence system voltage $V_{sn}\angle\phi_n$. As in the balanced case, one state y_h is then augmented for each harmonic of interest. The steady state solution of the harmonics are then found, solving (19) with the correspondingly modified $\hat{\mathbf{A}}$ matrices.

IV. Validation of Analytical Procedure

Results are validated by examining the VSC under both balanced and unbalanced operating conditions. Validation is carried out by comparing the results obtained from the analytical method with those obtained from a time domain

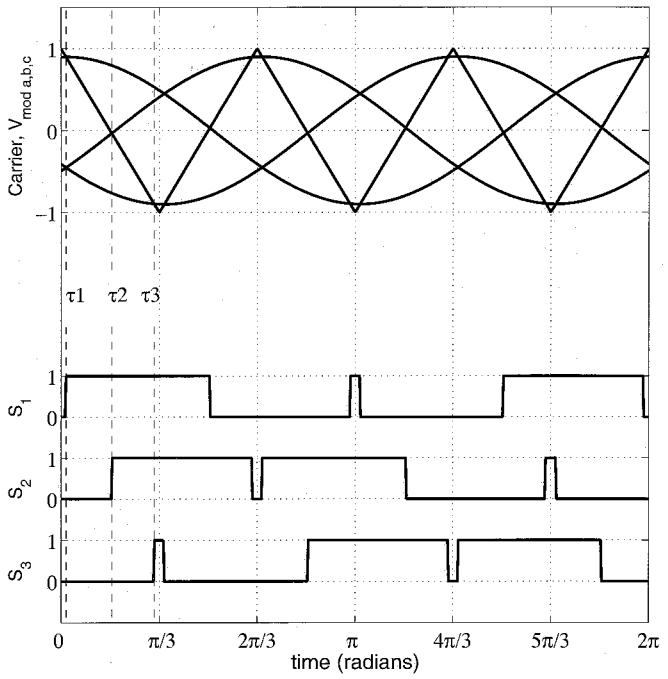

Fig. 5. SPWM gating pattern generation.

EMTDC/PSCAD simulation. For the purpose of validation, the carrier frequency is chosen to be 3 times the fundamental system frequency (i.e., $n = 1$); consistent with the carrier frequency used in very high power VSC-based FACTS equipment.

A. Balanced Operation

The VSC of Fig. 4 is operated using SPWM with a modulation index of $m_a = 0.9$ p.u. and a delay angle of $\delta = 3°$. A step by step application of the analytical procedure is presented.

1) The switching times associated with the given m_a and δ are found by comparing a triangle wave carrier of unit amplitude, with a three phase set of modulating signals. The modulating signals are

$$v_{\mathrm{mod}a}(t) = m_a \cos(\omega t - \delta)$$
$$v_{\mathrm{mod}b}(t) = m_a \cos(\omega t - 2\pi/3 - \delta)$$
$$v_{\mathrm{mod}c}(t) = m_a \cos(\omega t - 4\pi/3 - \delta).$$

They are shown in Fig. 5. For the case under study, the switching times are $\tau_1 = 0.0524$, $\tau_2 = 0.5404$, $\tau_3 = 0.9921$.

2) The steady state solution of the system is found as per [8]. For the case under study, the initial condition that yields a steady state solution is $i_{d\,ss} = 0.0434$ p.u., $i_{q\,ss} = 0.685$ p.u., $v_{dc\,ss} = 2.134$ p.u.

3) The states are augmented with one equation for each harmonic of interest. For this example, the harmonics of interest will be the ac current positive sequence fundamental, negative sequence 5th, and positive sequence 7th harmonics. Also, the average dc voltage on the capacitor and its 6th harmonic ripple will be found. The $\mathbf{H}$ and $\mathbf{M}$ matrices are

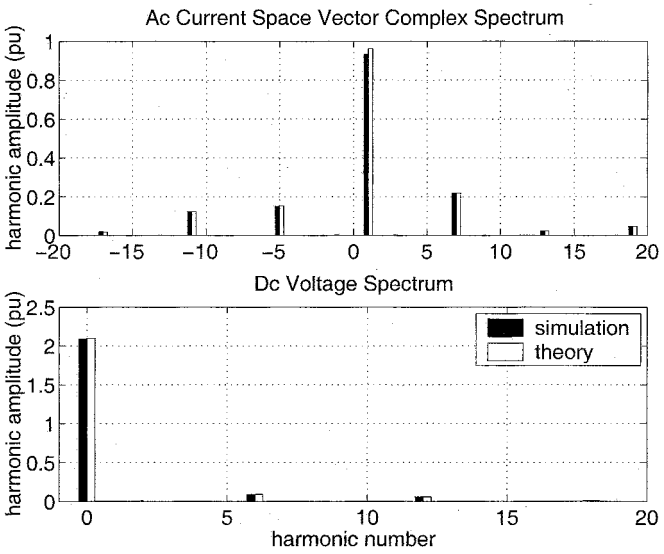

Fig. 6. Harmonic spectra under balanced operation.

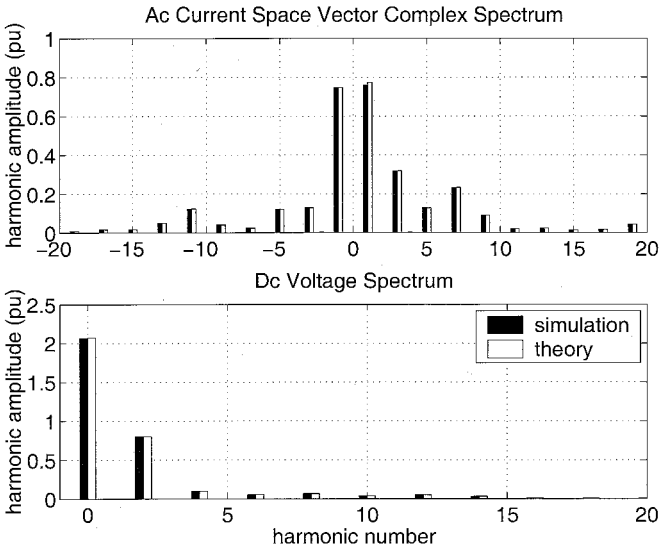

Fig. 7. Harmonic spectra with 0.1-p.u. negative sequence in firing signals.

$$\mathbf{H} = \begin{bmatrix} \frac{3}{\pi} e^{-j1\pi/3} & j\frac{3}{\pi} e^{-j1\pi/3} & 0 & 0 & 0 \\ \frac{3}{\pi} e^{j5\pi/3} & j\frac{3}{\pi} e^{j5\pi/3} & 0 & 0 & 0 \\ \frac{3}{\pi} e^{-j7\pi/3} & j\frac{3}{\pi} e^{-j7\pi/3} & 0 & 0 & 0 \\ 0 & 0 & \frac{3}{\pi} & 0 & 0 \\ 0 & 0 & \frac{3}{\pi} e^{-j6\pi/3} & 0 & 0 \end{bmatrix} \quad (23)$$

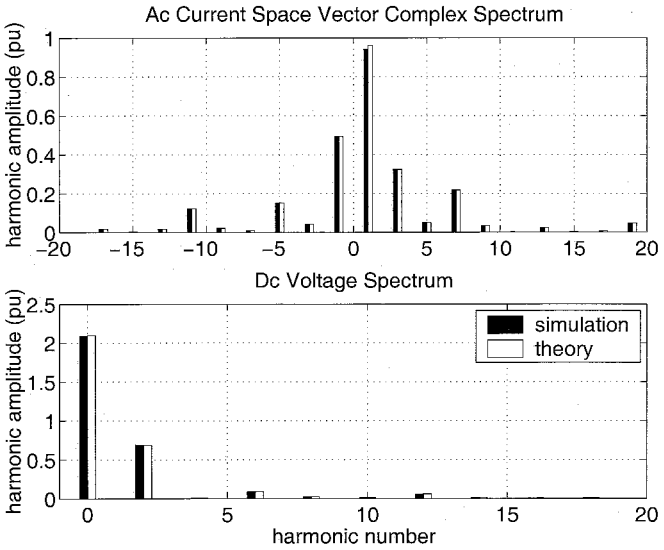

Fig. 8. Harmonic spectra with 0.1-p.u. negative sequence in system voltage.

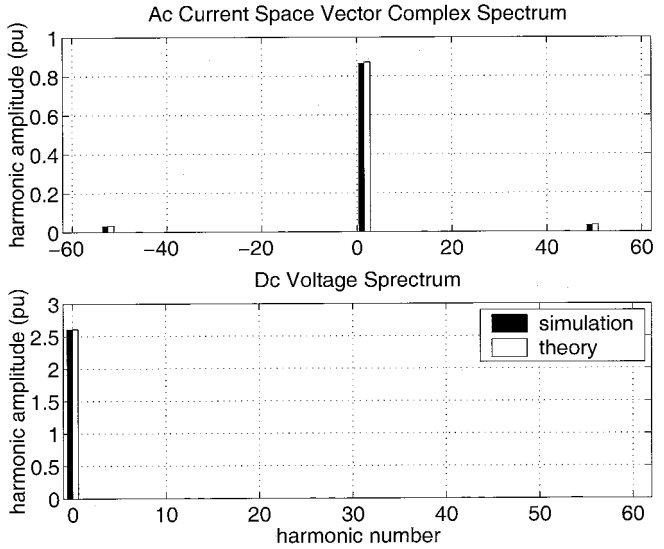

Fig. 9. Balanced steady state operation of a high switching frequency PWM converter.

$$\mathbf{M} = \begin{bmatrix} j1 & 0 & 0 & 0 & 0 \\ 0 & -j5 & 0 & 0 & 0 \\ 0 & 0 & j7 & 0 & 0 \\ 0 & 0 & 0 & 0 & 0 \\ 0 & 0 & 0 & 0 & j6 \end{bmatrix}. \tag{24}$$

The last two rows of the $\mathbf{H}$ and $\mathbf{M}$ matrices implements the dc voltage harmonic calculations. These will calculate the coefficient of the dc term and the $e^{j6\omega t}$ term in the complex Fourier series. This positive sideband term contains all of the information necessary to calculate the sixth harmonic component of the dc voltage.

4) Equation (18) is solved using the τ values found in step 1 and the associated initial condition found in step 2. For the case under study, the initial condition is

$$\hat{\mathbf{x}}(0) = [0.0434 \;\; 0.685 \;\; 2.134 \;\; V_s \;\; 0 \;\; 0 \;\; 0 \;\; 0 \;\; 0 \;\; 0] \tag{25}$$

where the system voltage is balanced with $v_{sa} = V_s \cos(\omega t)$ where $V_s = 1$ and $\omega = 1$.

The resulting harmonics are $\vec{I}^{+1} = 0.963$ p.u., $\vec{I}^{-5} = 0.152$ p.u., $\vec{I}^{+7} = 0.2181$ p.u., $V_{dc}^{0} = 2.10$ p.u., and $V_{dc}^{6} = 0.0452$ p.u.

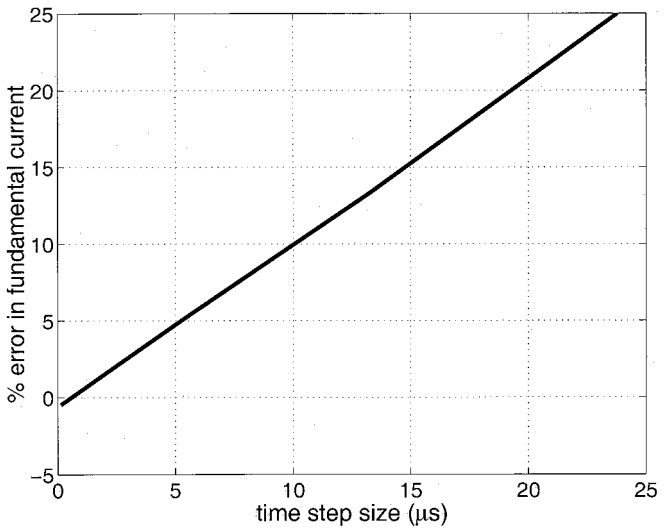

Fig. 10. Percent of error in the magnitude of fundamental frequency converter current as a function of simulation time step size.

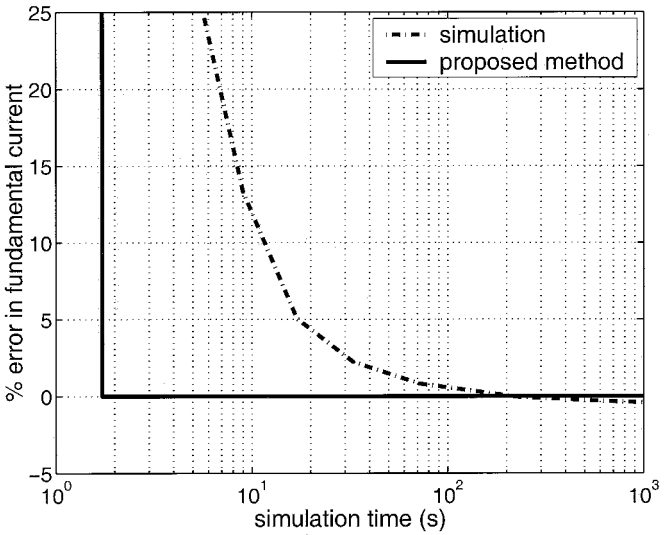

Fig. 11. Percent of error in the magnitude of fundamental frequency converter current as a function of simulation time.

The calculated harmonic spectrum of the current is compared with results from a PSCAD/EMTDC simulation in Fig. 6. Excellent agreement exists between the proposed analytical technique and simulation. The only perceptible difference occurs at fundamental frequency and stems from simulation error. Simulation errors result from the accumulation of integration errors from the trapezoidal algorithm and minor inaccuracies in interpolation of the switching instants. These errors may be minimized through reduction of the simulation time step; however, a corresponding increase in simulation time will result.

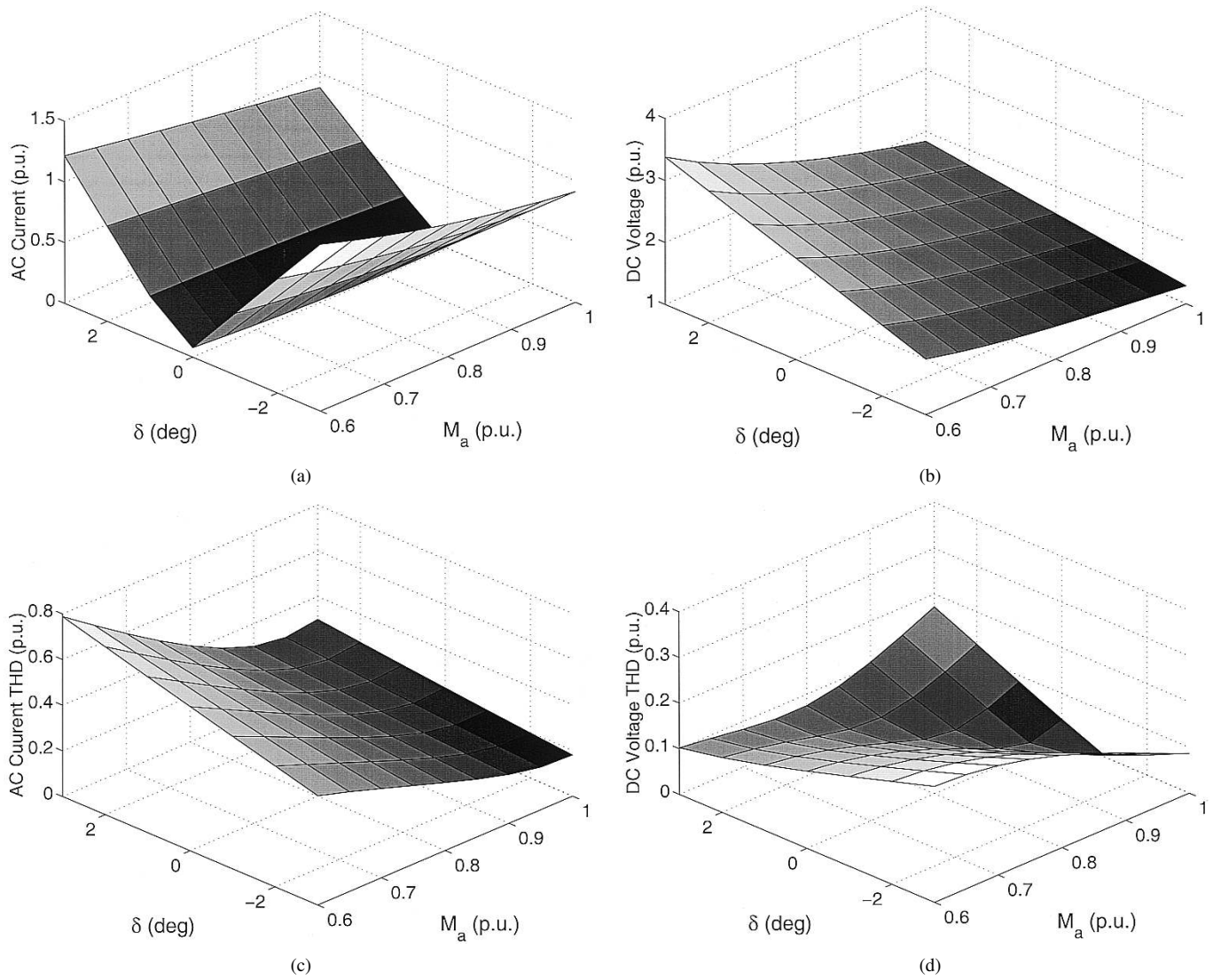

Fig. 12. Balanced steady state operation. (a) Fundamental ac current. (b) Average dc voltage. (c) THD in ac current. (d) THD in dc voltage.

B. Operation Under Unbalanced Gating

In the previous section, the modulating signals were balanced three phase signals of 0.9-p.u. amplitude, lagging the system voltage by $\delta = 3°$. In this section, a 0.1-p.u. amplitude negative sequence component (of zero phase) is added yielding modulating signals of

$$v_{\mathrm{mod}a}(t) = 0.9\cos(\omega t - \delta) + 0.1\cos(\omega t)$$
$$v_{\mathrm{mod}b}(t) = 0.9\cos(\omega t - 2\pi/3 - \delta) + 0.1\cos(\omega t + 2\pi/3)$$
$$v_{\mathrm{mod}c}(t) = 0.9\cos(\omega t - 4\pi/3 - \delta) + 0.1\cos(\omega t + 4\pi/3).$$

Analytical and simulation results are compared in Fig. 7. Again, excellent agreement between the proposed theory and simulation exists. All uncharacteristic harmonics, such as negative sequence fundamental, and positive and negative sequence third harmonic, are correctly identified. On the dc bus, uncharacteristic harmonics including the second and fourth are also identified.

C. Operation Under Unbalanced Voltage

A 0.1-p.u. negative sequence voltage is superimposed on the system voltage, while balanced firing is maintained with a modulation index of 0.9 p.u. and a delay angle of 3°. The system voltage is therefore given by

$$v_{sa}(t) = 1\cos(\omega t) + 0.1\cos(\omega t)$$
$$v_{sb}(t) = 1\cos(\omega t - 2\pi/3) + 0.1\cos(\omega t + 2\pi/3)$$
$$v_{sc}(t) = 1\cos(\omega t - 4\pi/3) + 0.1\cos(\omega t + 4\pi/3).$$

Analytical and simulation results are compared in Fig. 8.

Comparing the results of this section with those of the previous section, shows that the VSC steady state solution and harmonics respond quite differently to imbalance in system voltage than to imbalance in firing. In both cases, a similar 10% negative sequence imbalance was introduced.

V. Implementation Efficiency

Although the proposed analytical procedure offers a closed form solution for the harmonic analysis of a VSC, the number

of necessary matrix exponential evaluations becomes large if a high frequency PWM converter is analyzed. For harmonic analysis of a VSC operating at a carrier frequency of $3n$ times, the system fundamental frequency $6n+2$ matrix exponentials need to be evaluated: $3n+1$ are required for obtaining the steady state solution, and $3n+1$ are required for the harmonic analysis.

To ascertain the computational efficiency of implementing the proposed technique when n is large, a VSC operating at a carrier frequency of 51 times the system fundamental frequency ($n = 17$). This represents a switching frequency of 3.06 kHz on a 60-Hz network. The converter is operated with a delay angle of 1° and a modulation index of 0.9 p.u. All other system parameters are left unchanged, and are given in the Appendix. Characteristic harmonics of the ac current and the dc voltage are calculated up to the 60th harmonic. The resulting harmonic spectra are given in Fig. 9. Once again, simulation results closely match those obtained by implementing the proposed procedure, assuming a sufficiently small time step is employed and the system is simulated for a sufficiently long duration to settle into steady state.

In simulation, a tradeoff exists between desired accuracy and computation time, since high accuracy will require use of a small simulation time step. Fig. 10 plots the percent error in fundamental frequency ac current magnitude as the time step size is varied. From the figure, it may be seen that the simulation error is approximately proportional to the time step size.

Clearly, appropriate initialization of the simulation is required if the circuit is to rapidly settle into a steady state. Appropriate initialization of the dc capacitor voltage on the STATCOM simulation model allows steady state operation to be achieved after ten to 20 cycles of the fundamental. Fig. 11 shows the relation between simulation time and the percent error in fundamental frequency ac current magnitude. The STATCOM is simulated for 15 cycles in PSCAD/EMTDC (on a 1-GHz, Pentium III, Windows 2000 workstation). Notice that the simulation results converge to a slightly erroneous solution with -0.65% error. This residual error stems, to a large part, from the fact that initialization transients have not fully decayed to zero in the allotted 15 cycles.

Also shown in Fig. 11 is the time required to execute the proposed procedure. The procedure is implemented as an un-compiled MATLAB script which executes in 1.7 s (on the same 1-GHz, Pentium III, Windows 2000 workstation). As may be observed from Fig. 11, the proposed technique offers significant improvement in accuracy and reduction in simulation time compared with brute force simulation; even if the converter switching frequency is high.

The proposed technique achieves a target error below 1% approximately two orders of magnitude faster than brute force simulation. Equally important, in contrast to simulation, accurate results may be obtained without the need of error analysis, optimal selection of time step size, or estimation of how many cycles must be simulated before steady state is truly reached.

VI. Application Example

This section employs the proposed procedure to calculate the total harmonic distortion current injected into a transmission system by a STATCOM as a function of operating point. The voltage ripple on the dc bus is simultaneously calculated, as it may be used to rate the dc storage capacitor.

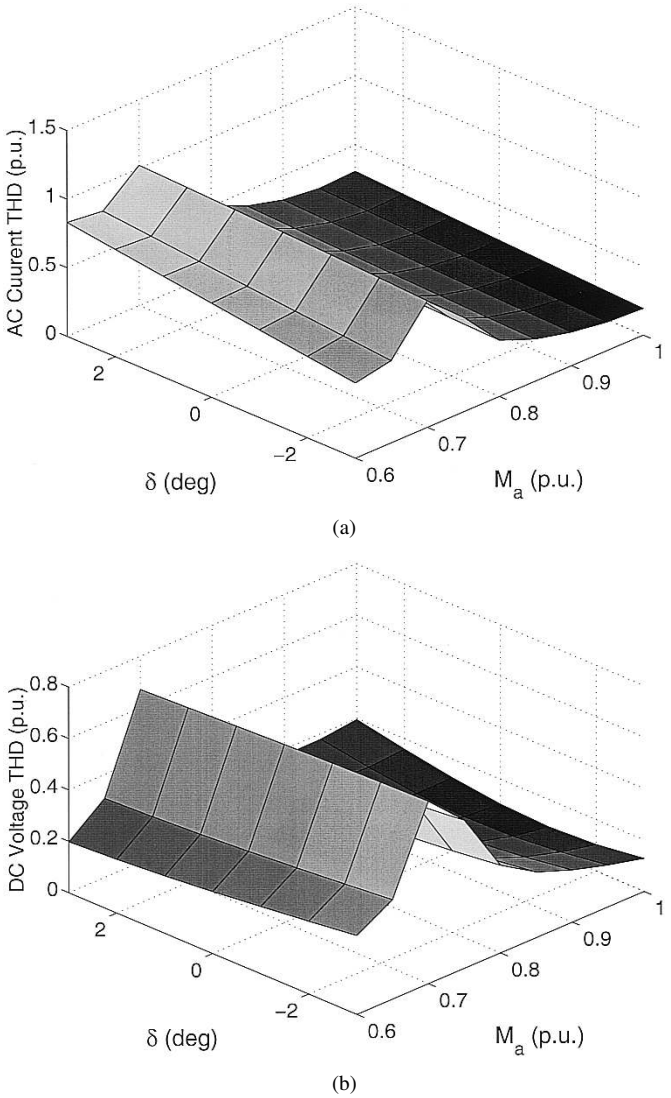

Fig. 13. Operation with 2% system voltage imbalance. (a) THD in ac current. (b) THD in dc voltage.

The operating point of the STATCOM is specified in terms of the modulation index m_a and phase angle δ of the SPWM modulating signals. The resulting fundamental frequency ac current and average dc voltage are shown in Fig. 12(a) and (b). Note that for $\delta < 0$ degrees, the ac current is inductive, while for $\delta > 0$ degrees, the current is capacitive.

The total harmonic current distortion is calculated from the complex spectrum

$$THD = \sqrt{\sum_{n=-30}^{n=+30} \left(\vec{I}^{n}\right)^2 - \left(\vec{I}^{+1}\right)^2}. \tag{26}$$

The total harmonic distortion on the dc voltage is also calculated from the first 30 harmonics. The harmonic distortion on the current and voltage are shown in Fig. 12(c) and (d).

The harmonic distortions are in line with expectations. DC THD is low over the entire operating range. AC current THD

TABLE I
SYSTEM DATA

System Data	Per Unit Values
$R = 0.02\ \Omega$	$R = 0.02\ p.u.$
$L = 0.20\ H$	$X_L = 0.20\ p.u.$
$C = 0.50\ F$	$X_C = 2.00\ p.u.$
$V_{sa} = 1/\sqrt{2}\ V$	$V_{sa} = 1.00\ p.u.$
$V_{dc}^0 = 2.1\ V$	$V_{dc}^0 = 2.1\ p.u.$
$\omega = 1.00\ rad/s$	$\omega = 1.00\ p.u.$
$V_{base} = 1/\sqrt{2}\ V$	
$I_{base} = 1/\sqrt{2}\ A$	
$Z_{base} = 1\ \Omega$	
$S_{base} = 3/2\ VA$	
$\omega_{base} = 1.00\ rad/s$	

become large only if a high average dc voltage level is combined with a small modulation index (i.e., when $m_a = 0.6$ p.u. and $\delta = +3^\circ$). Since this range of operation is not typically utilized in any STATCOM application, it is of little concern.

Fig. 13 shows the dc voltage and ac current THD when a modest 2% negative sequence voltage component exists on the system. Even this small level of voltage imbalance is seen to drastically alter the THD curves. In particular, an exceptionally high ac and dc THD will now exist if the STATCOM is operated at a modulation near 0.7 p.u. The local maximum in THD is a result of strong ac-dc side coupling at this modulation index. The local maximum occurs within the range of operation utilized by most STATCOMs that operate with sinusoidal pulse width modulation.

By comparing Fig. 12 with Fig. 13, it may be concluded that even very modest system voltage imbalance must be accounted for when rating the dc capacitor of a STATCOM or when calculating its harmonic injection into the network.

VII. CONCLUSIONS

An analytical method for calculating the ac and dc side harmonics of a VSC is presented. The technique uses a direct solution of the steady state followed by a direct solution of the VSC harmonics, thus avoiding the numerical errors and convergence problems associated with iterative methods. Furthermore, the proposed method is capable of calculating all uncharacteristic harmonics associated with the operation of a VSC under unbalanced system voltage or unbalanced inverter firing conditions. Comparison of analytical results with those obtained from EMTDC/PSCAD validate the proposed method in all cases. The technique is applied to the harmonic analysis of a STATCOM.

APPENDIX

The data used for system parameters are summarized below. Note that the same base values for voltage and current are used on both the ac and dc sides of the converter as shown in Table I.

REFERENCES

[1] A. Gole, "Steady state frequency response of statcom," *IEEE Trans. Power Delivery*, vol. 16, pp. 18–23, Jan. 2001.
[2] M. Madrigal and E. Acha, "Modeling of custom power equipment using harmonic domain techniques,", vol. 1, pp. 264–269, 2000.
[3] S. Dong, W. Zhonghong, J. Chen, and Y. Song, "Harmonic resonance phenomena in statcom and relationship to parameter selection of passive components," *IEEE Trans. Power Delivery*, vol. 16, pp. 46–52, Jan. 2001.
[4] C. Schauder and H. Mehta, "Vector analysis and control of advanced static VAR compensators," *Proc. Inst. Elect. Eng.*, pt. C, vol. 140, pp. 299–306, July 1993.
[5] I. Papic and A. Gole, "Steady state frequency response of the unified power flow controller,", vol. 1, pp. 526–531, 2002.
[6] N. Mohan, T. Undeland, and W. Robbins, *Power Electronics*, 2nd ed. New York: Wiley, 1995.
[7] E. Clarke, *Circuit Analysis of AC Power Systems*. New York: Wiley, 1943.
[8] P. Lehn, "Exact modeling of the voltage source converter," *IEEE Trans. Power Delivery*, vol. 17, pp. 217–222, Jan. 2002.
[9] H. Visser and P. van den Bosch, "Modeling of periodically switched networks," in *IEEE Power Electron. Specialists Conf.*, 1991, pp. 67–73.

Peter W. Lehn (M'99) received the B.Sc. and M.Sc. degrees in electrical engineering from the University of Manitoba, Winnipeg, in 1990 and 1992, respectively. He received the Ph.D. degree from the University of Toronto, ON, Canada, in 1999.

Currently, he is an Assistant Professor at the University of Toronto. From 1992 to 1994, he was with the Network Planning Group of Siemens AG, Erlangen, Germany.